Author/s:
Bellis, J;Duluc, I;Romagnolo, B;Perret, C;Faux, MC;Dujardin, D;Formstone, C;Lightowler, S;Ramsay, RG;Freund, JN;De Mey, JR

Title:
The tumor suppressor Apc controls planar cell polarities central to gut homeostasis

Date:
2012-08-01

Citation:
Bellis, J., Duluc, I., Romagnolo, B., Perret, C., Faux, M. C., Dujardin, D., Formstone, C., Lightowler, S., Ramsay, R. G., Freund, J. N. & De Mey, J. R. (2012). The tumor suppressor Apc controls planar cell polarities central to gut homeostasis. Journal of Cell Biology, 198 (3), pp.331-341. https://doi.org/10.1083/jcb.201204086.

Persistent Link:
https://hdl.handle.net/11343/264851

The tumor suppressor *Apc* controls planar cell polarities central to gut homeostasis

Julien Bellis,[1,3] Isabelle Duluc,[2,3] Béatrice Romagnolo,[4] Christine Perret,[4] Maree C. Faux,[5] Denis Dujardin,[1,3] Caroline Formstone,[6] Sally Lightowler,[7] Robert G. Ramsay,[7,8,9] Jean-Noël Freund,[2,3] and Jan R. De Mey[1,3]

[1]Laboratoire de Biophotonique et Pharmacologie, Unité Mixte de Recherche 7213, Centre National de la Recherche Scientifique, 67401 Illkirch, France
[2]Institut National de la Santé et de la Recherche Medicale U682, 67200 Strasbourg, France
[3]Université de Strasbourg, 67081 Strasbourg, France
[4]Institut Cochin, Institut National de la Santé et de la Recherche Medicale U567, 75014 Paris, France
[5]Ludwig Institute for Cancer Research, Parkville, Victoria 3050, Australia
[6]Medical Research Council Centre for Developmental Neurobiology, King's College London, London SE1 1UL, England, UK
[7]Peter MacCallum Cancer Centre, Melbourne, Victoria 3002, Australia
[8]Sir Peter MacCallum Department of Oncology and [9]Department of Pathology, The University of Melbourne, Parkville, Victoria 3052, Australia

The stem cells (SCs) at the bottom of intestinal crypts tightly contact niche-supporting cells and fuel the extraordinary tissue renewal of intestinal epithelia. Their fate is regulated stochastically by populational asymmetry, yet whether asymmetrical fate as a mode of SC division is relevant and whether the SC niche contains committed progenitors of the specialized cell types are under debate. We demonstrate spindle alignments and planar cell polarities, which form a novel functional unit that, in SCs, can yield daughter cell anisotropic movement away from niche-supporting cells. We propose that this contributes to SC homeostasis. Importantly, we demonstrate that some SC divisions are asymmetric with respect to cell fate and provide data suggesting that, in some SCs, mNumb displays asymmetric segregation. Some of these processes were altered in apparently normal crypts and microadenomas of mice carrying germline *Apc* mutations, shedding new light on the first stages of progression toward colorectal cancer.

Introduction

Intestinal epithelia exhibit extraordinary tissue renewal. In the small intestine (SI) and colon crypt base columnar (Cheng and Leblond, 1974), Lgr5^{hi} cells (Barker et al., 2007) at positions 1–6 represent proliferating stem cells (SCs) interdigitated with CD24^{+} and/or cKit^{+} niche-supporting cells (Sato et al., 2011; Rothenberg et al., 2012).

Invariant asymmetric SC division with divisions generating one SC and one transit amplifying/progenitor cell with occasional symmetric divisions compensating for SC losses has long been considered central for crypt homeostasis (Booth and Potten, 2000). However, recent data suggest that SC fate is regulated stochastically by populational asymmetry (Lopez-Garcia et al., 2010; Snippert et al., 2010). This yielded a model in which (a) equipotent Lgr5^{hi} SCs undergo neutral competition for contact with niche-supporting cells, (b) SC loss is compensated by symmetric self-renewal of a neighboring SC, and (c) differentiation occurs when cells lose the short-range signals for SC competence from the niche (Snippert et al., 2010; Simons and Clevers, 2011). Yet, this model seems at odds with data suggesting that a variety of early committed progenitors in or above position 5 generate specialized cell types (Bjerknes and Cheng, 1999), which migrate up or down from the common origin (Bjerknes and Cheng, 1981). Accordingly, the dividing Lgr5^{hi} cells at positions 1–6 should be a mix of SCs and progenitor cells. Of note, committed progenitors are thought to be able to revert to full SC competence, making reversibility of cellular decisions key elements to intestinal organization (Buske et al., 2011).

The balance between SC renewal and fate is perturbed by mutations in the *adenomatous polyposis coli* (*APC*) tumor suppressor gene in humans and *Apc*$^{Mutant/+}$ mice, whereby loss of

J.-N. Freund and J.R. De Mey contributed equally to this paper.

Correspondence to Jan R. De Mey: jan.de-mey@unistra.fr

Abbreviations used in this paper: ACF, aberrant crypt foci; APC, adenomatous polyposis coli; BP, basal process; EdU, 5-ethynyl-2′-deoxyuridine; LOBA, longitudinally oriented basal asymmetry; LOH, loss of heterozygosity; MIP, maximal intensity projection; OCD, oriented cell division; PCP, planar cell polarity; SC, stem cell; SI, small intestine; wt, wild type.

The Rockefeller University Press $30.00
J. Cell Biol. Vol. 198 No. 3 331–341
www.jcb.org/cgi/doi/10.1083/jcb.201204086

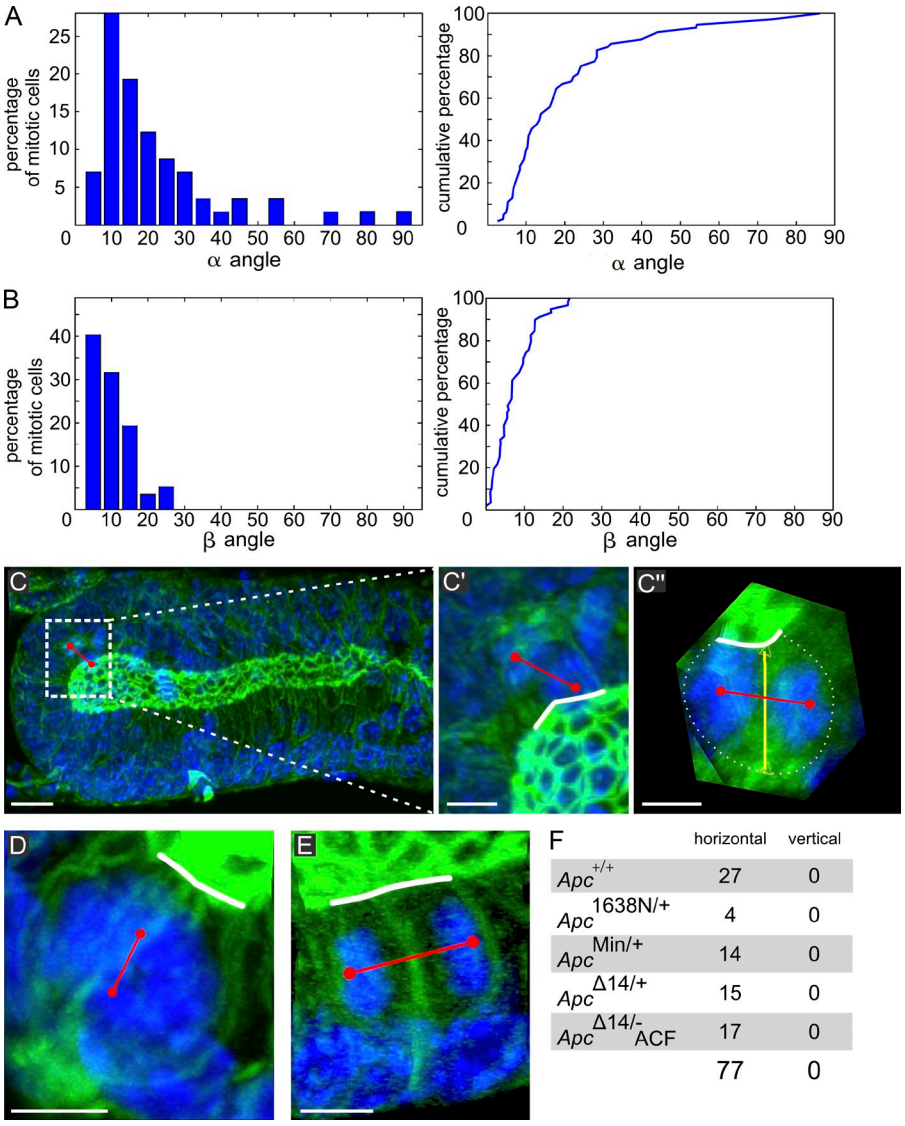

Figure 1. **Spindle orientation in the tubular part and the semispherical parts of colon crypts.** (A and B, left) α and β angles in 67 mitotic cells in wt crypts of six animals. (A and B, right) Cumulated percentages: 80% of α angles are ≤30°, but ∼20% display angles up to 90°. Nearly 100% of β angles are ≤20°. (C) MIP of optical sections of a crypt comprising a telophase. (C′ and C′′) Zoomed-in images of the region of interest defined by the dotted rectangle in C, where C′′ is 3D rotated to display the spindle axis perpendicular to the observer. Red line shows spindle axis; white line shows apical surface; yellow line links the center of apical surface and basal pole. In C′, the spindle appears nearly perpendicular to the apical surface, whereas C′′ shows it is in fact parallel (complete 3D examination shown in Video 2). (D) MIP of a prometaphase displaying a spindle axis perpendicular to the apical surface (3D viewing shown in Video 3). (E) MIP of a telophase in an $Apc^{Min/+}$ mouse with the spindle parallel to the apical surface. (F) Number of meta/telophases at the crypt base exhibiting horizontal versus vertical spindle orientation in wt ($Apc^{+/+}$), $Apc^{1638N/+}$, $Apc^{Min/+}$, and $Apc^{\Delta 14/+}$ crypts and in ACF of $Apc^{\Delta 14/-}$ mice ($Apc^{\Delta 14/-}$ ACF). Bars: (C) 10 µm; (C′–E) 5 µm.

the wild-type (wt) allele (loss of heterozygosity [LOH]) initiates microadenomas formation (Wasan et al., 1998). SC-specific loss of *Apc* triggers microadenoma formation (Barker et al., 2009). In cultivated cells, *APC* mutations induce a range of mitotic defects (Green et al., 2005; Draviam et al., 2006; Dikovskaya et al., 2007). In vivo, normal-appearing SI crypts of $Apc^{Min/+}$ mice display alterations in spindle orientation and cytokinesis of transit-amplifying cells, which are held responsible for delamination (Fleming et al., 2009), tetraploidy (Caldwell et al., 2007), and loss of vertical spindle reorientation in $Lgr5^{hi}$ SCs (Quyn et al., 2010). Thus, mitotic defects are considered among the first detectable alterations predisposing to cancer initiation (Pease and Tirnauer, 2011). Yet, such drastic/immediate changes are difficult to reconcile with the slow progression toward colon cancer.

Finally, important differences exist between the SI and colon at the histological, developmental, and genetic levels (Chang and Nadler, 1975; Bjerknes and Cheng, 1981; Altmann, 1990; Rothenberg et al., 2012). Thus, there is a need to better understand these processes in the distal colon, the major site of cancer in humans.

Results and discussion

We challenged the current models of crypt homeostasis and perturbation by *Apc* mutations with a high-resolution topological study of the mouse descending colon. We first analyzed spindle orientation and accompanying cell shape changes during the mitotic cycle by 3D imaging of entire crypts (Fig. S1, C and D; and Videos 1 and 2). Metaphase through telophase spindle orientation was determined in the tubular part by measuring two angles referring to planar (the β angle between the spindle axis and the apical pole) and longitudinal (the α angle between the spindle and longitudinal crypt axes) orientation (Fig. S1, A and B; Gong et al., 2004). Like in the SI (Fleming et al., 2007), spindles always planarly align with the apical cell surface (β < 20°); in addition, 80% longitudinally align with the crypt axis (α < 30°; Fig. 1, A and B), thus fulfilling the criteria of oriented cell division (OCD; Strutt, 2005). At the crypt bottom, where the cells are disposed semispherically, even if serial optical sections might sometimes suggest vertical spindle reorientation, complete 3D visualization showed that, in reality, it was horizontal in 100% of the cases (Fig. 1, C–C′′ and F; and Video 3).

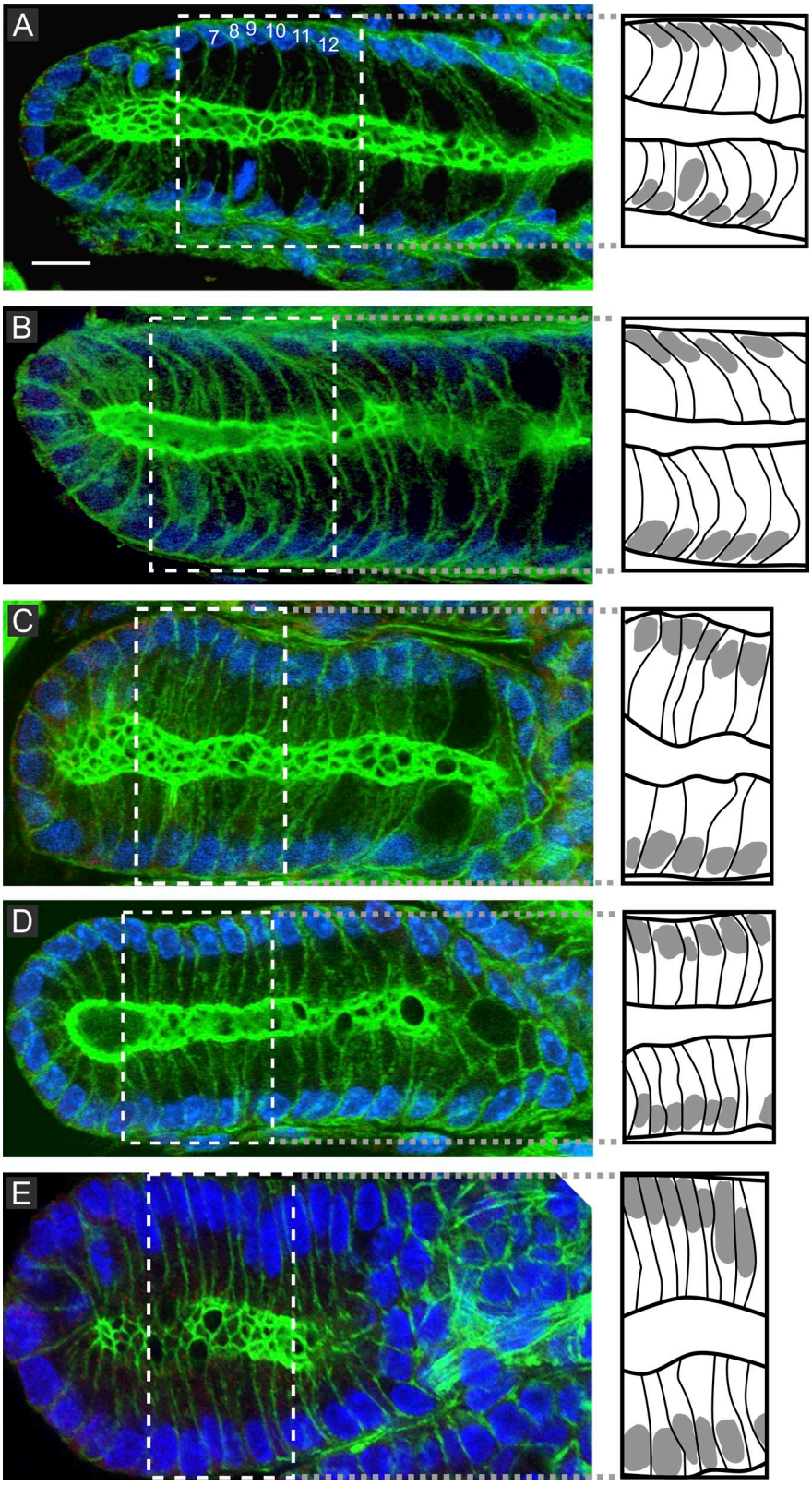

Figure 2. **LOBA in interphase cells of wt and *Apc*$^{mutant/+}$ mice.** (A) LOBA is identified as a bent shape toward the crypt bottom in wt mice (see also Fig. 3 A). The numbers represent the cell numbering relative to the crypt bottom, where cell Nr 1 is located. (B–E) It is intact in two thirds (B) and lost in one third (C) of *Apc*$^{\Delta 14/+}$ crypts, in 80% of *Apc*$^{Min/+}$ crypts (D), and in all ACF of *Apc*$^{\Delta 14/+}$ mice (E). The dotted white lines define the region of interest drawn in the boxes to the right, linked by grey dotted lines. Bar, 5 µm.

Cells displaying a nearly vertical spindle axis were restricted to prometaphases (Fig. 1 D and Video 4) when spindle position is not yet definitive (Fleming et al., 2007). This rules out a mechanism of SC division associated with vertically reorienting the spindle (Quyn et al., 2010).

In the tubular part ($n = 48$), we uncovered a novel expression of planar cell polarity (PCP), designated here as longitudinally oriented basal asymmetry (LOBA) and characterized by all interphase cells being bent at their base, uniformly oriented toward the crypt bottom (Fig. 2 A). Like in the SI (Fleming et al., 2007),

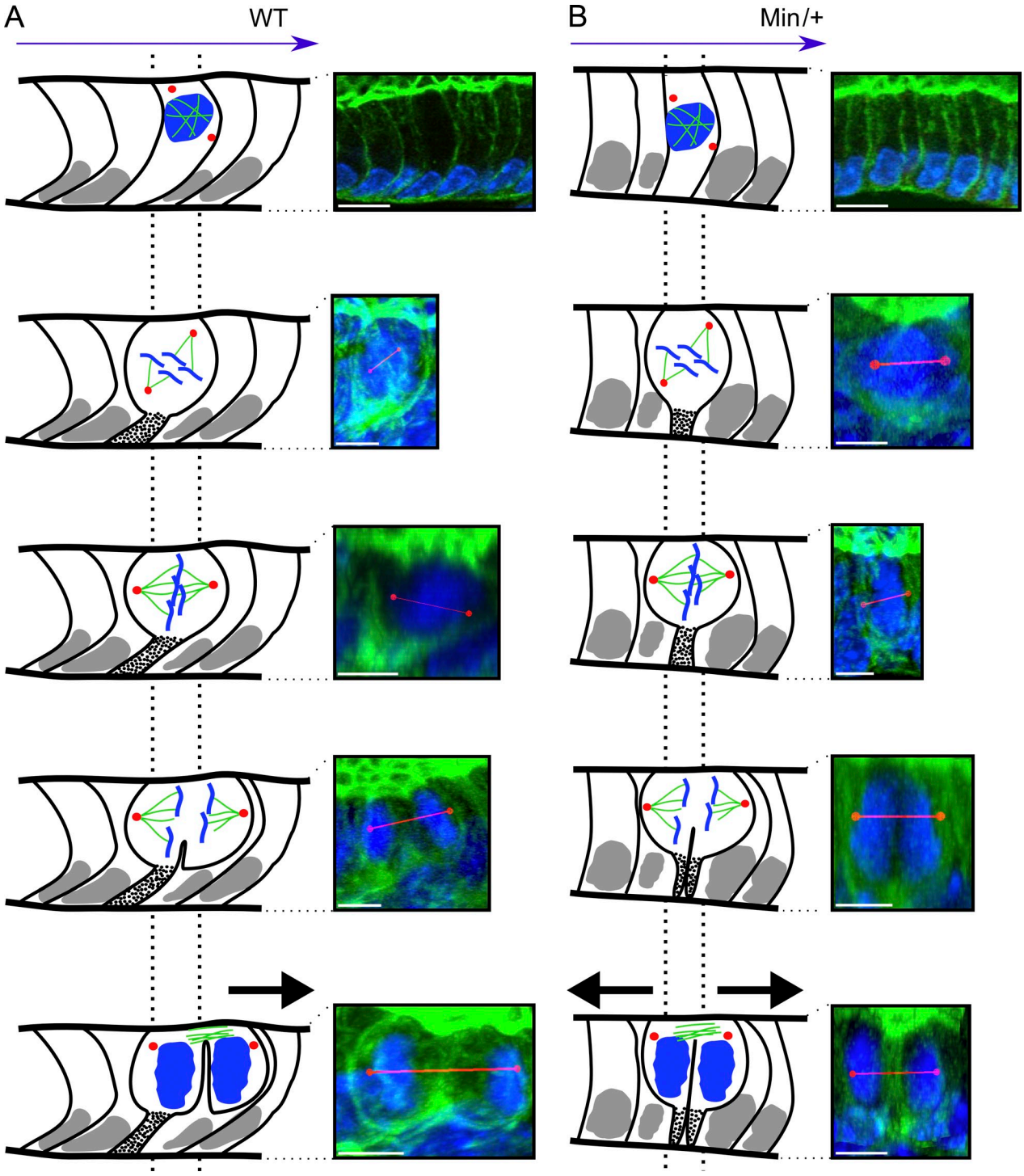

Figure 3. **The LOBA/OCD unit generates anisotropic daughter cell movement that is lost in $Apc^{Min/+}$ crypts.** Dotted lines delineate the original cell position relative to the daughters. (A) In wt crypts exhibiting LOBA, mitotic cells maintain a BP (dotted stalk) uniformly bent toward the crypt bottom. Whenever a dividing cell exhibits longitudinal spindle orientation (80% of the cases), only the daughter closest to the crypt base inherits the BP, whereas the other moves one position upwards (black arrow). (B) In LOBA$^-$ $Apc^{Min/+}$ crypts, the BP is positioned centrally such that both daughters inherit it, abolishing anisotropic movement (black arrows). Bars: (A and B, first row) 10 µm; (A and B, bottom images) 5 µm. Red lines indicate the spindle axis.

dividing cells remained connected to the underlying lamina by an F-actin–rich basal process (BP). As in interphase, it was bent toward the crypt base (Fig. 3 A and Video 5). Consequently, in the 80% of cells displaying longitudinal spindle orientation (small α angle), the cleavage furrow sets up in front of the BP, anchoring the daughter cell closest to the crypt bottom, unlike its sister (Fig. 3 A). During anaphase B spindle elongation, the apical pole elongated in the same direction so that the nonattached daughter moved up one position (Fig. 3 A). Conversely, in cells aligning the spindle along the crypt circumference (large α angle), the BP had been bisected and inherited by both daughters, who apparently moved in opposite directions (Videos 2 and 6).

At the crypt bottom, cells exhibited LOBA only when approaching the tubular part, but like elsewhere in the crypt, they kept a BP. In half of the ana/telophases (8/15), the BP asymmetrically segregated in one daughter but was cleaved and segregated symmetrically in both daughters in the other half (Fig. S3, A and B).

This comprehensive topological view reveals that OCD and LOBA form a novel functional unit that orchestrates daughter cell placement and anisotropic movements. It provides a mechanism for the mitotic pressure on adhering neighbors previously described (Chang and Leblond, 1971, 1974). In the tubular part of the crypt, it is expected to contribute to the upward cell migration but also to circumferential cell positioning that fixes the crypt diameter (Simons and Walz, 2006). The involvement of LOBA/OCD in cell movement is supported by data showing that cells moved slower at the crypt base, where LOBA is displayed less (Chang and Nadler, 1975).

Intestinal SCs give rise to two lineages, absorptive and secretory, and an earlier study in the descending colon indicated that the latter become committed in the lower part of the SC niche (Chang and Nadler, 1975). To further investigate this, we compared the appearance of Atoh1/Math1 in the nuclei of sister cell doublets by immunostaining crypts fixed 6 or 8 h after a 5-ethynyl-2′-deoxyuridine (EdU) pulse. Atoh1 commits an activated progenitor of the secretory cell lineage and has a role in crypt homeostasis (Yang et al., 2001; Shroyer et al., 2007). 6 and 8 h after the EdU pulse, Atoh1^{+} nuclei made up 15–20% of the nuclei at positions 1–16, and of these, 15% were positive for EdU. 20% of all the doublets (n = 220) were Atoh1$^{+/+}$ (Fig. 4, A and A′, stars). Atoh1^{+} cells in M phase were also seen regularly (unpublished data). 6 h after the EdU pulse, of >200 scored doublets, no Atoh1$^{+/-}$ asymmetry was detected. In contrast, 8 h after the EdU pulse, a subset of doublets, all located at the crypt bottom (positions 1–4) and representing 5% of the doublets at this position (n = 142), unambiguously exhibited asymmetric Atoh1$^{+/-}$ distribution (Fig. 4, C–D′′; and Videos 7 and 8). The slender shape of these cells indicates that they were undifferentiated. These observations indicated that the Atoh1$^{+/-}$ cells arose from Atoh1^{-} cells in which one sister started expressing Atoh1 some time after completion of cell division. It remains theoretically possible that some Atoh1$^{+/+}$ doublets may arise from Atoh1^{-} cells, but our study does not address this. We next tested whether Muc2, a marker of mucous-secreting cells, exhibits asymmetric expression in sister cell doublets. 8 h after the EdU pulse, numerous Muc2$^{+/+}$ doublets and Muc2^{+} mitotic cells were seen at positions 1–10 (Fig. 4 B), but not a single Muc2$^{+/-}$ doublet was seen in >400 scored. Muc2$^{+/+}$ doublets and mitoses (Fig. 4 B, arrow) contained moderate amounts of Muc2 and, therefore, correspond to mucous cells maturing into goblet cells. Interestingly, 20% of the cells at the crypt base (positions 1–4) were mature Muc2^{+} and EdU^{-}, perhaps corresponding to the Muc2^{+}/cKit^{+} crypt base goblet cells (Rothenberg et al., 2012). They were interdigitated with Muc2^{-}/EdU^{+} cells, which likely are Lgr5^{hi} cells. We conclude that in the colon SC niche, SC divisions asymmetric with respect to cell fate occur. Such divisions are considered as asymmetric.

To address whether SC mitoses can yield cells committed to differentiation directly through asymmetric mitosis, we investigated the distribution of proteins involved in it (Neumüller and Knoblich, 2009). Celsr1 (Fig. S2, A′ and B′) and Vangl2 (Fig. S2 D′) were associated with the basolateral plasma membrane. In dividing cells, even at the crypt base, there was no indication of asymmetric distribution for Celsr1 (Fig. S2 C′) or Vangl2 (not depicted) nor to their linker to the spindle apparatus positioning machinery, NuMA (Fig. 5 A′ and Fig. S2 C′′; Morin and Bellaïche, 2011). Thus, according to these markers, all divisions would be symmetrical. We then studied mNumb, an evolutionarily conserved cell fate determinant, which in several SC types displays asymmetric segregation as a cortical crescent adjacent to one spindle pole (Gulino et al., 2010). Four well-characterized anti-mNumb antibodies (Zhong et al., 1996; Dho et al., 1999, 2006; Rasin et al., 2007) all visualized mNumb in association with vesicular structures densely lining the basolateral plasma membrane or located in the cytoplasm of interphase cells (Fig. 5, A and C–E), as in radial glial cells (Rasin et al., 2007) and MDCK cells (Dho et al., 2006), and double labeling with antibodies raised against the center or C terminus of mNumb revealed ∼50% overlap (Fig. 5, C–E). In anaphases, both antibodies labeled vesicular structures accumulating in the spindle midzone (Fig. 5, C–C′′′). Importantly, in 60% of the telophases located predominantly in the SC niche (below position 6), these structures segregated asymmetrically into only one daughter, where they became densely packed at the side of the reassembling nucleus facing the cleavage furrow (Fig. 5, A, B [right], D, and E; and Videos 9 and 10). They may contain a dedicated isoform or state of mNumb recognized by the two unrelated antibodies with different efficiency. The absence of asymmetric cortical segregation of mNumb, Vangl1, Celsr1, and NuMA indicates an absence of a mechanism that coordinates spindle orientation and cell fate determinants as used in invertebrates (Neumüller and Knoblich, 2009). Strengthening the view that these observed asymmetric segregations are of functional significance, in 75% of the cases (12/16) in which mNumb-containing vesicles had asymmetrically distributed in one daughter, this daughter also had inherited asymmetrically the BP.

We next assessed the role of APC in LOBA/OCD and mNumb segregation. Both longitudinal (α angle) and planar (β angle) spindle alignments were severely affected in *Apc*$^{fl/fl}$ × *Villin-CreER*^{T2} mice after conditional knockout in the adult gut (Fig. S1, E–H). Spindle orientation, however, was unaffected in the normal-appearing crypts of three *Apc*$^{Mutant/+}$ models (Fig. S1, E–H): *Apc*$^{1638N/+}$, considered to be *Apc* haploinsufficient, and *Apc*$^{Min/+}$ and *Apc*$^{\Delta 14/+}$, which coexpress wt APC and APC truncations. This is at odds with previous data (Caldwell et al., 2007; Fleming et al., 2009), probably because of our measurement of two angles as compared with only one in these studies. In the tubular part of crypts from *Apc*$^{\Delta 14/+}$ aberrant crypt foci (ACF), longitudinal, but not planar, alignment was affected (Fig. S1, E–H), and consequently, crypts were enlarged (Fig. 2 E). At the crypt base, the spindles also remained planarly aligned (Fig. 1, E and F). Thus, OCD depends on *Apc* but is not altered until LOH, the longitudinal component being more dependent on *Apc* than the planar one. Loss of OCD is correlated with an increased crypt diameter and irregular shape,

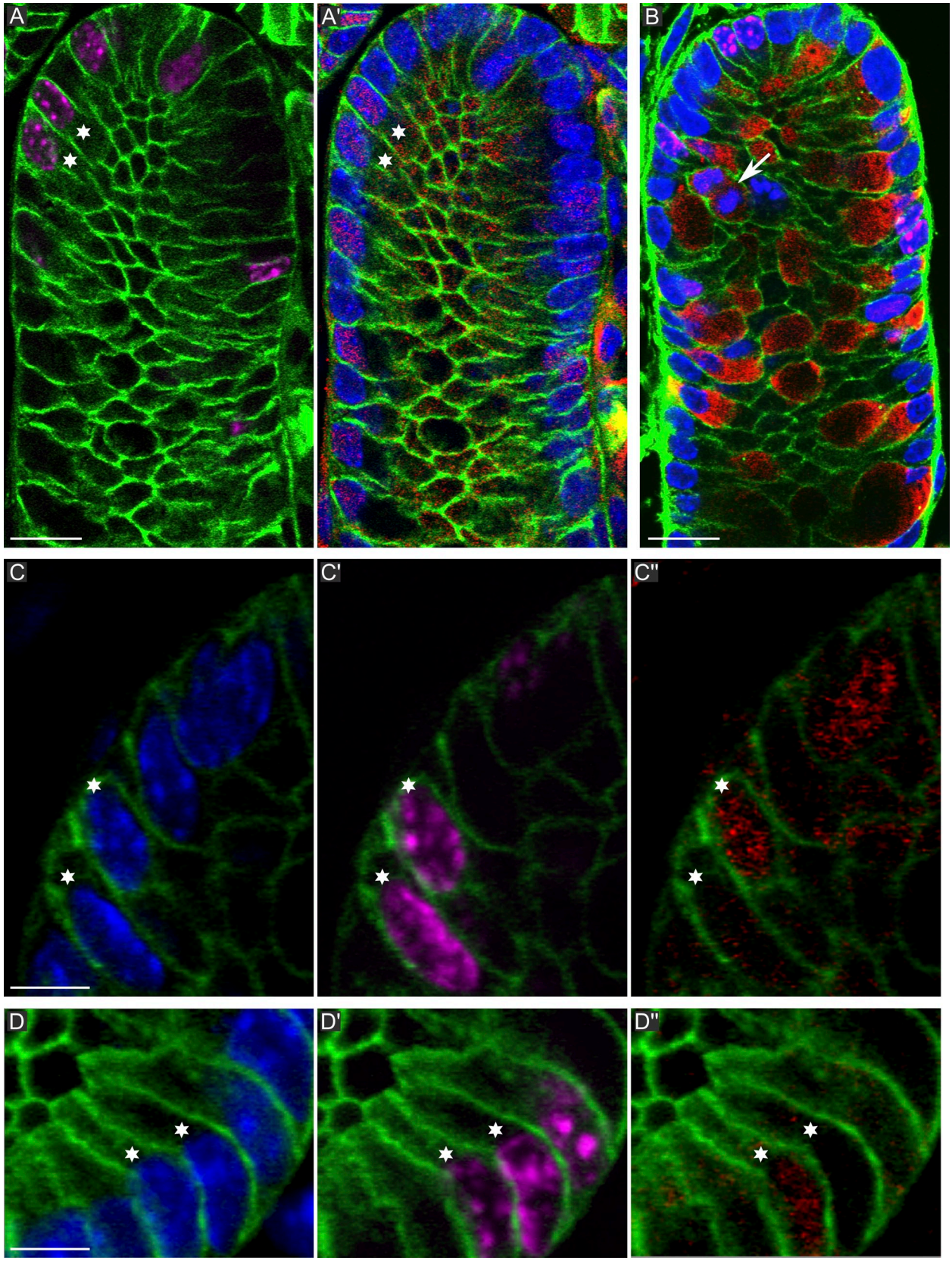

Figure 4. **Atoh1 and Muc2 doublet sister cell analysis.** (green) β-Catenin; (magenta) EdU; (blue) DAPI. (A and A′) Distribution of EdU and Atoh1 (red) in a section grazing the crypt lumen. The marked doublet is Atoh1$^{+/+}$. (B) Muc2 (red) and EdU. Muc2^{+} cells contain varying amounts of mucin. The arrow indicates a dividing Muc2^{+} cell. (C–D′′) EdU marked doublets showing one Atoh1^{+} and one Atoh1^{-} sister (see also Videos 8 and 9). In D–D′′, only one of three doublets is shown (marked by stars). The others are visible in Video 9. The data shown are from a single representative experiment out of three repeats. Bars: (A and B) 10 µm; (C and D) 5 µm.

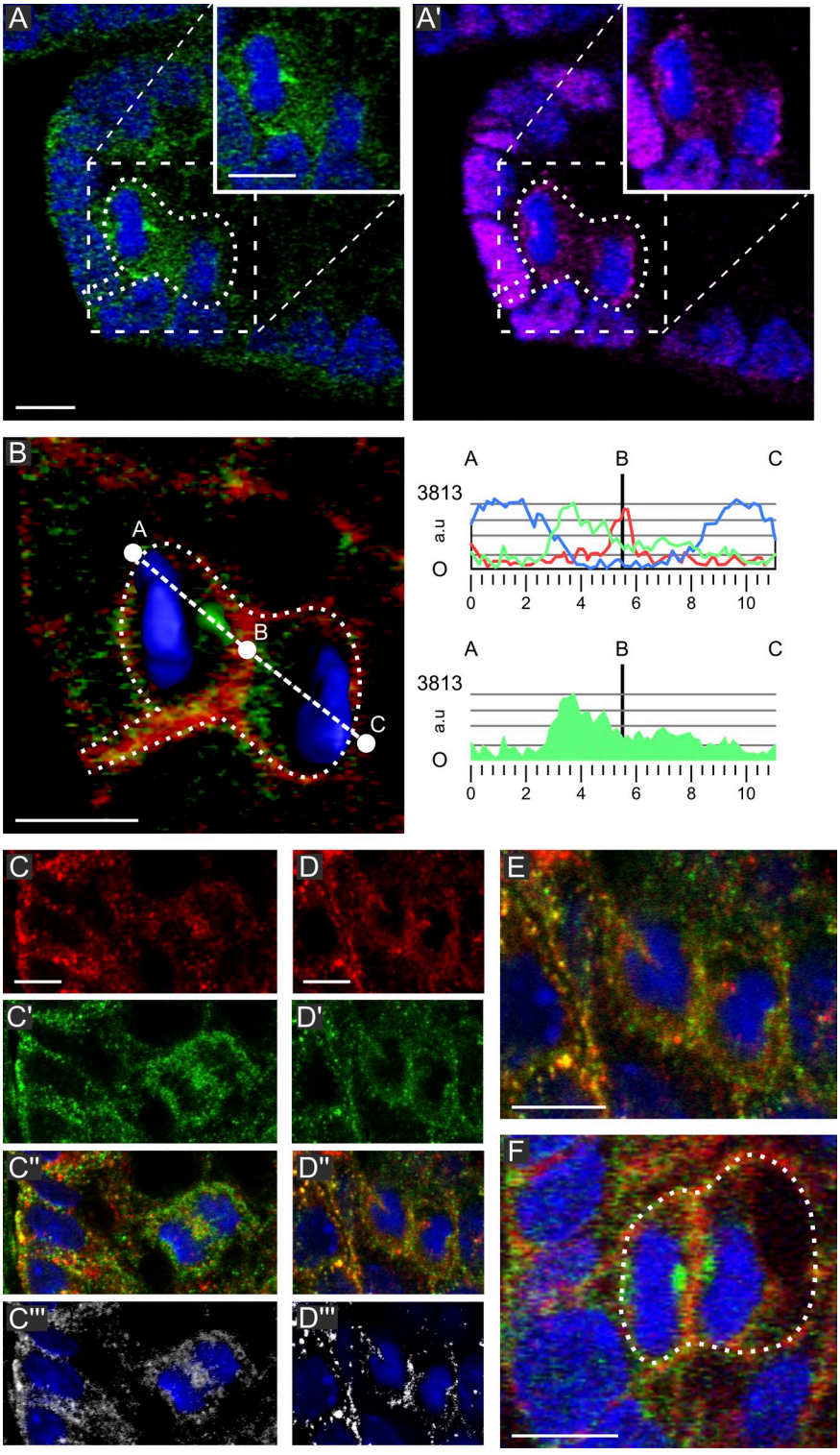

Figure 5. **Symmetric NuMA and asymmetric mNumb segregation.** (A and A′) Telophase at position 3 in a wt crypt with asymmetrically segregating mNumb-containing vesicles (green) but two NuMA cortical crescents (magenta). The insets show the cell of interest without dotted lines. (B) Higher magnification (left) and fluorescence quantification (right) through the A–C line for mNumb (green), actin (red), and DAPI (blue). (C–E) mNumb signals of a rabbit anti–amino acids 489–522 (red) and a guinea pig anti–C terminus of mNumb (green); the rabbit antibody recognizes these more efficiently. (C–C′′′) Anaphase: mNumb containing vesicles accumulating in the spindle midzone; both antibodies label these structures as illustrated by the colocalization signal (C′′′). (D–E) Telophase: mNumb containing vesicles segregating into one of the daughters. (F) $Apc^{\Delta 14/+}$ crypt: a telophase at position 4 with symmetric mNumb segregation whereby accumulations of vesicles are seen at each side of the cleavage furrow. The data shown are from a single representative experiment out of three repeats. The dotted lines delineate the cell of interest. Bars, 5 µm. a.u., arbitrary unit.

reminiscent of the altered OCD in polycystic kidney disease (Fischer et al., 2006).

In contrast to the bent shape kept in interphase cells of $Apc^{1638N/+}$ crypts (n = 26; not depicted), one third of $Apc^{\Delta 14/+}$ crypts (n = 80), the majority of $Apc^{Min/+}$ crypts (80%, n = 43), and all ACF from $Apc^{\Delta 14/+}$ mice (n = 9) had lost LOBA (Fig. 2), demonstrating dependency upon *Apc*, noteworthy before LOH. These LOBA$^-$ crypts were clustered, and in all telophases, the BP was positioned centrally and segregated symmetrically into both daughters, which moved in opposite directions (Fig. 3 B), in line with the decreased cell migration reported in $Apc^{Min/+}$ mouse crypts (Mahmoud et al., 1997). At the crypt base, the frequency of asymmetric BP inheritance is also reduced in *Apc* mutants (Fig. S3, C and D). Asymmetric mNumb segregation was reduced in LOBA$^+$ $Apc^{\Delta 14/+}$ crypts and further dropped in LOBA$^-$ crypts (Fig. 5 F and Table 1).

Table 1. **Quantification of asymmetric mNumb segregation in wt and LOBA$^+$ and LOBA$^-$ *Apc*$^{\Delta 14/+}$ crypts**

Crypt types	Cell positions	*n*	Asymmetric	Symmetric	Percentage of asymmetric
wt	1–6	31	19	12	61.2
wt	>6	20	4	16	20
Δ14LOBA$^+$	1–6	18	7	11	38
Δ14LOBA$^+$	>6	15	0	15	0
Δ14LOBA$^-$	1–6	12	2	10	16.6
Δ14LOBA$^-$	>6	5	0	5	0

Thus, this reduction represents a very early molecular event in crypts with monoallelic mutations of *Apc*, with further loss when crypts become LOBA$^-$. The early perturbations of LOBA/OCD and mitotic mNumb behavior are predicted to affect SC renewal and progenitor kinetics in the SC niche.

Our data show the existence of SC division with asymmetric cell fate for the secretory lineage (Atoh1$^{+/-}$ doublets) near the crypt base, in line with previous data (Chang and Nadler, 1975), and uncover a new type of asymmetric segregation of the cell fate determinant, mNumb in 50% of the cells of the SC niche, with a directional bias toward the cell remaining attached by a BP. Thus, the SC niche comprises niche-supporting cells and a population of Lgr5^{hi} cells made of SCs and progenitors. They also strongly indicate that novel tissue/PCPs described here play a central role in adult colon crypt homeostasis. Given the recent discovery of cKit$^+$ Goblet cells with Paneth-like SC-stimulating function (Rothenberg et al., 2012), we propose in the SC niche that anisotropic daughter cell movements driven by LOBA/OCD contribute to the probability of one daughter cell to divide away from the CD24$^+$/cKit$^+$ niche-supporting cell to which its mother was contacting. This migrating-away daughter thus becomes a committed precursor of one lineage, whereas the remaining daughter keeps contact with the niche-supporting cell and remains parked within the crypt base. Committed progenitors can fully regain SC competence by encountering a niche-supporting cell. By introducing anisotropic daughter cell movements instead of spindle reorientation in SCs (Quyn et al., 2010), our model provides an alternative mechanism for the concept of neutral competition of SCs for niche-supporting cells, which is central to the concept of stochastic population asymmetry (Klein and Simons, 2011).

The functional relevance of the symmetric/asymmetric distribution of mNumb remains unknown. A regulator of Notch, it may impact this pathway to influence SC fate and lineage specification (van Es et al., 2005; Fre et al., 2011), like in the developing thymus (Aguado et al., 2010) and in the interfollicular adult epidermis (Clayton et al., 2007). These SC divisions too look symmetric by all current topological criteria but are in reality asymmetric with respect to cell fate. In embryonic muscle progenitor cells, however, Numb can modulate both self-renewal and commitment in a context-dependent manner during a lineage progression (Jory et al., 2009). In addition, mNumb controls other pathways and cell functions than Notch (Gulino et al., 2010), leaving open additional ways to specify subpopulations of SCs or downstream progenitors. For instance, mNumb regulates p53, which in mammary SCs is very important to their expansion (Colaluca et al., 2008).

Importantly, we identify so far unrecognized processes, the anisotropic movements of daughter cells in the SC niche and the asymmetric mNumb segregation, as very dependent on *Apc* and show that spindle orientation, previously believed to be very dependent, is less so. The subtle and gradual nature of the effects reported here during the sequence of *Apc* alterations (monoallelic mutation and LOH) parallels the slow progression toward cancer. These findings underscore that future functional studies will have to be interpreted within the complex, 3D, and dynamic cytological framework characteristic of intestinal crypts.

Materials and methods

Mice models

wt, *Apc*$^{Min/+}$ (provided by P. Héry, Commissariat à l'énergie atomique et aux énergies alternatives, Saclay, France; Su et al., 1992), *Apc*$^{\Delta 14/+}$ (Colnot et al., 2004), *Apc*$^{1638N/+}$ (Fodde et al., 1999), and *Apc*$^{fl/fl}$ × *Villin-CreER*^{T2} (Andreu et al., 2005) mice were housed according to the guidelines of the Ethic Committee of the University of Strasbourg.

Preparation of colon and SI samples

For experiments assaying proliferation and sister cell doublets, EdU was injected intraperitoneally (10 mg/ml in PBS and 10 µl/g of body weight) 6 or 8 h before animals were killed. Mice were anesthetized and euthanized before dissection. The distal colon or jejunum segments were opened and immediately washed with a solution of warm (37°C) PHEM (60 mM Pipes, 25 mM Hepes, 10 mM EGTA, and 2 mM $MgCl_2$). The tissue was pinned on a wax surface and fixed for 40 min at RT in 3% paraformaldehyde in PHEM supplemented with 15 µM taxol. During fixation, it was processed into small fragments. These were then rinsed three times in PBS and stored at 4°C in PBS/NaN_3. For microadenoma (ACF) isolation, the colon was fixed as previously stated in this paragraph and incubated with methylene blue. Microadenomas were visualized by trans-illumination and extracted with fine needles. Using two thin needles, the muscle lining was removed, and thin slices containing two to three rows of crypts were resected. All subsequent steps were performed in an Eppendorf tube. Samples were treated with PBS containing, successively, 200 µM NH_4Cl for 1 h, 3% sodium deoxycholate for 1 h, and 0.5% Triton X-100 for 30 min and subsequently blocked for 30 min in PBS/BSA 1%/Triton X-100 0.2%. For labeling with anti-Atoh1, antigen retrieval was performed by incubating the sample in 0.1 mM sodium citrate buffer, pH 6.0, at 95°C for 30 min before blocking in PBS/BSA 1%/Triton X-100 0.2%.

Immunolabeling of intact crypts

Primary and secondary antibody dilutions were made in the same solution. Incubation with first antibodies in 1 ml was performed for 2 h at RT followed by overnight at 4°C. After rinsing three times, they were incubated twice during 4 h with secondary antibodies (containing phalloidin-Alexa Flour 568), first at RT and then at 4°C. They were rinsed three times, incubated in DAPI (5 µl of a 1-mg/ml stock solution in 10 ml of PBS) for 20 min, and rinsed in PBS. They were deposited on a slide in a drop of PBS. The PBS was removed to leave the fragments collected in the middle almost dry. They were mounted in 30 µl mounting medium (ProLong Gold; Molecular Probes) and covered by a coverslip. The primary antibodies used were the following: human autoantibodies against γ-tubulin and NuMA (1:1,000), 1 µg/ml affinity-purified rabbit

anti-mNumb against a synthetic peptide containing amino acids 489–522 of mNumb (provided by Y. Jan, Howard Hughes Medical Institute, University of California, San Francisco, San Francisco, CA; Zhong et al., 1996; Aguado et al., 2010), 1 µg/ml rabbit and guinea pig anti-mNumbC against the C terminus of mNumb, rabbit anti-mNumbA against the center of mNumb (provided by J. McGlade, University of Toronto, Toronto, Ontario, Canada; Dho et al., 1999, 2006), 1 µg/ml rabbit anti-Celsr1 raised against the most membrane-proximal region of the Celsr1 cytoplasmic tail (Formstone et al., 2010), 1 µg/ml rabbit anti-Vangl2 (provided by M. Montcouquiol, Institut F. Magendie des Neurosciences, Institut National de la Santé et de la Recherche Medicale, Bordeaux, France; Montcouquiol et al., 2008), rabbit anti-Muc2, and rabbit anti-Atoh1 (gift of J. Johnson, University of Texas Southwestern Medical Center, Dallas, TX; Helms and Johnson, 1998). For those experiments using anti-Atoh1 or Muc2 antibodies, the cell borders were labeled using a mouse monoclonal against β-catenin. EdU was detected using the cell proliferation assay (Click-iT; Invitrogen) according to manufacturer's instructions. Antigen retrieval (for labeling Atoh1), permeabilization, and immunostaining were performed first followed by the EdU detection step and, finally, DAPI staining.

Fast confocal microscopy

Fast confocal microscopy images were collected using a 63×, NA 1.4 lens on a scanning confocal microscope (SP5; Leica) in bidirectional resonance mode (8,000 Hz), with 8× averaging/plane/per channel. DAPI and Alexa Fluor 647 were detected simultaneously, and Alexa Fluor 488 and 568 (or 555) were detected sequentially. An acquisition typically consisted of 60 planes × 4 channels with a z step of 0.5 µm and a pixel size of 141 nm.

Spindle orientation measurements

Using Imaris software (Bitplane), image stacks were processed for isosurface rendering and 3D mark positioning (Fig. S1 D). Mitotic staging was performed according to DAPI and γ-tubulin signals. The strong actin signal at the apical adhesion belt was used to determine the longitudinal axis of the crypt over a short distance at the level of each mitotic figure (typically 12 µm; Fig. S1, A and B, yellow). Using the 3D measuring points function, the γ-tubulin–labeled spindle poles were marked, and a red line connecting them visualized the spindle axis. Next, a line (Fig. S1 A, gray) linking the center of the spindle axis (Fig. S1, A and B, orange) and crossing the crypt axis orthogonally was calculated. The α angle is the absolute smallest angle between the spindle axis and the crypt axis and was calculated from the projection of the spindle and crypt axes on plane 1 (Fig. S1 B). The β angle is the smallest absolute angle between the spindle axis and the apical pole and was calculated from the projection of the same axes on plane 2, perpendicular to plane 1 and parallel to the crypt axis (Fig. S1 B). Measurements were made on metaphases/telophases, during which spindle orientation determines the cleavage plane (Reinsch and Karsenti, 1994; Fleming et al., 2007). All calculations were performed with a custom-written MATLAB (MathWorks).

Error estimation

To estimate the possible error made on angle measurements, four mitoses found in four different crypts were measured four times, and we calculated the SD for each mitoses and the mean SD. The SD ranged from 0.3 to 1.5° with a mean value of 0.7° for the α angle and from 0.6 to 1.7° with a mean value of 0.9° for the β angle. As such, these small error measurement values have no consequences for the interpretation of our results, including where small angles are calculated.

Accuracy of crypt long axis determination in crypts with irregular inner lumen

In wt crypts, the orientation of the crypt long axis is determined over a segment of 12 µm. However, the inner lumen of crypts in ACF of $Apc^{\Delta 14/+}$ mice and of $Apc^{fl/fl}$ × *Villin-CreERT2* mice is quite irregular. We therefore assessed whether here, too, this is a suitable determinant of crypt long axis orientation by comparing α angle measurement in an $Apc^{fl/fl}$ × *Villin-CreERT2* crypt using a local versus a global crypt axis. We found that a global axis did not change α angle measurements because comparison of the results obtained on α angle measurement performed in a series of 17 cells with either the local axes or the global axis showed no major differences.

3D viewing of individual mitotic cell and sister cell doublets

For creating 3D rotations of a whole mitotic cell or a volume comprising a sister cell doublet of interest, an image stack of a volume encompassing it was created using the Imaris 3D cropping function. As before, using the 3D measuring points function, the γ-tubulin–labeled spindle poles were marked, and a red line connecting them visualized the spindle axis. In cases in which spindle orientation with respect to the apical surface was not clear right away, a yellow line connecting the middle of the apical pole with the basal one was incorporated into the stack (Fig. 1, C–C′′). Viewing 3D rotations of the F-actin signal combined with these axes allowed determining spindle axis orientation and, subsequently, the cleavage plane orientation with respect to the apical–basal cell polarity. For studying BP formation and inheritance, cells in the crypt half touching the coverslip were used because the image quality here was optimal. EdU^+ sister cell doublets were easily recognized by their similar EdU content and speckled distribution in serial optical sections and especially in animations of 3D reconstructions of their surroundings. The latter were systematically used for doublets suspected to exhibit asymmetric Atoh1. The person doing the scoring had gained extensive experience from scoring $Atoh^{+/+}$ and $Muc^{+/+}$ EdU^+ sister doublets. Even so, doublets that presented even a slight uncertainty were removed from the dataset. In crypts of the SI, EdU and antibody labeling worked as well, but because the proliferating cells were too crowded, the technique could not be used reliably. In certain cases, the centers of nuclear doublets were also linked by a red line to facilitate 3D viewing (Video 9).

Statistical analysis

Data were expressed as mean values ± SD of the number of measurements. The statistical significance between experimental models was assessed by the unpaired Student's *t* test using R software whereby $P < 0.05$ was considered to be statistically significant.

Online supplemental material

Fig. S1 demonstrates that imaging of intact colon crypts and analysis of spindle orientation by measuring angles α and β in wt and *Apc* mutant mice show normal OCD in crypts from $Apc^{1638N/+}$, $Apc^{Min/+}$, and $Apc^{\Delta 14/+}$ mice but perturbation upon sudden loss of *Apc* in crypts of floxed *Apc* × *Villin-CreERT2* mice treated with tamoxifen, isolated 5 d after tamoxifen administration, and upon LOH in ACF of $Apc^{\Delta 14/+}$ mice. Fig. S2 shows distribution of PCP proteins in colon crypts. Fig. S3 shows inheritance of the BP in dividing cells of the crypt bottom. Video 1 shows animated optical sections through intact crypts flat mounted on a coverslip. Video 2 shows animated maximal intensity projection (MIP) tilt series of the optical sections through a crypt comprising a telophase at position 5 displaying a large (>80°) α angle. Video 3 shows animated MIP tilt series of the cell in position 3 of the crypt in Fig. 1 A and depicted in Fig. 1 (C′ and C′′). Video 4 shows animated MIP tilt series of the prometaphase in Fig. 1 E. Video 5 shows animated MIP tilt series of a metaphase at position 5 after positioning it upright shows LOBA of a BP. Video 6 shows animated MIP tilt series of the cell in Video 1. Video 7 shows 3D animation of the $Atoh1^{+/-}$ doublet sister cells shown in Fig. 5 (C–C′′). Video 8 shows animation of optical sections and 3D of the $Atoh1^{+/-}$ doublet sister cells shown in Fig. 5 (D–D′′). Video 9 shows animation of optical sections through the telophase at position 3 shown in Fig. 4 (A and B). Video 10 shows 3D animation of the telophase shown in Fig. 4 (A and B) and Video 6. Online supplemental material is available at http://www.jcb.org/cgi/content/full/jcb.201204086/DC1.

Part of this work is the thesis work of J. Bellis for obtaining the Ph.D. degree of the University of Strasbourg.

P. Héry provided the $Apc^{Min/+}$ mice. We are indebted for the gift of antibodies to Y. Jan and J. McGlade (mNumb), J. Johnson (Atoh1), and M. Montcouquiol (Vangl1). Thanks go to the members of the imaging facilities of the Centre de Recherche de Biochimie Macromoléculaire (Montpellier) and especially the Institut de la Génétique et de la Biologie Moléculaire et Cellulaire (Illkirch) and to B. Baum and S. Robine for discussions and critical reading of the manuscript.

Support was given to J. Bellis by the Ligue Contre le Cancer and to R.G. Ramsay and M.C. Faux by the National Health and Medical Research Council, Australia.

Submitted: 16 April 2012
Accepted: 26 June 2012

References

Aguado, R., N. Martin-Blanco, M. Caraballo, and M. Canelles. 2010. The endocytic adaptor Numb regulates thymus size by modulating pre-TCR signaling during asymmetric division. *Blood.* 116:1705–1714. http://dx.doi.org/10.1182/blood-2009-10-246777

Altmann, G.G. 1990. Renewal of the intestinal epithelium: new aspects as indicated by recent ultrastructural observations. *J. Electron Microsc. Tech.* 16:2–14. http://dx.doi.org/10.1002/jemt.1060160103

Andreu, P., S. Colnot, C. Godard, S. Gad, P. Chafey, M. Niwa-Kawakita, P. Laurent-Puig, A. Kahn, S. Robine, C. Perret, and B. Romagnolo. 2005. Crypt-restricted proliferation and commitment to the Paneth cell lineage following Apc loss in the mouse intestine. *Development*. 132:1443–1451. http://dx.doi.org/10.1242/dev.01700

Barker, N., J.H. van Es, J. Kuipers, P. Kujala, M. van den Born, M. Cozijnsen, A. Haegebarth, J. Korving, H. Begthel, P.J. Peters, and H. Clevers. 2007. Identification of stem cells in small intestine and colon by marker gene Lgr5. *Nature*. 449:1003–1007. http://dx.doi.org/10.1038/nature06196

Barker, N., R.A. Ridgway, J.H. van Es, M. van de Wetering, H. Begthel, M. van den Born, E. Danenberg, A.R. Clarke, O.J. Sansom, and H. Clevers. 2009. Crypt stem cells as the cells-of-origin of intestinal cancer. *Nature*. 457:608–611. http://dx.doi.org/10.1038/nature07602

Bjerknes, M., and H. Cheng. 1981. The stem-cell zone of the small intestinal epithelium. III. Evidence from columnar, enteroendocrine, and mucous cells in the adult mouse. *Am. J. Anat.* 160:77–91. http://dx.doi.org/10.1002/aja.1001600107

Bjerknes, M., and H. Cheng. 1999. Clonal analysis of mouse intestinal epithelial progenitors. *Gastroenterology*. 116:7–14. http://dx.doi.org/10.1016/S0016-5085(99)70222-2

Booth, C., and C.S. Potten. 2000. Gut instincts: thoughts on intestinal epithelial stem cells. *J. Clin. Invest.* 105:1493–1499. http://dx.doi.org/10.1172/JCI10229

Buske, P., J. Galle, N. Barker, G. Aust, H. Clevers, and M. Loeffler. 2011. A comprehensive model of the spatio-temporal stem cell and tissue organisation in the intestinal crypt. *PLOS Comput. Biol.* 7:e1001045. http://dx.doi.org/10.1371/journal.pcbi.1001045

Caldwell, C.M., R.A. Green, and K.B. Kaplan. 2007. APC mutations lead to cytokinetic failures in vitro and tetraploid genotypes in *Min* mice. *J. Cell Biol.* 178:1109–1120. http://dx.doi.org/10.1083/jcb.200703186

Chang, W.W.L., and C.P. Leblond. 1971. Renewal of the epithelium in the descending colon of the mouse. I. Presence of three cell populations: vacuolated-columnar, mucous and argentaffin. *Am. J. Anat.* 131:73–99. http://dx.doi.org/10.1002/aja.1001310105

Chang, W.W.L., and N.J. Nadler. 1975. Renewal of the epithelium in the descending colon of the mouse. IV. Cell population kinetics of vacuolated-columnar and mucous cells. *Am. J. Anat.* 144:39–56. http://dx.doi.org/10.1002/aja.1001440104

Cheng, H., and C.P. Leblond. 1974. Origin, differentiation and renewal of the four main epithelial cell types in the mouse small intestine. I. Columnar cell. *Am. J. Anat.* 141:461–479. http://dx.doi.org/10.1002/aja.1001410403

Clayton, E., D.P. Doupé, A.M. Klein, D.J. Winton, B.D. Simons, and P.H. Jones. 2007. A single type of progenitor cell maintains normal epidermis. *Nature*. 446:185–189. http://dx.doi.org/10.1038/nature05574

Colaluca, I.N., D. Tosoni, P. Nuciforo, F. Senic-Matuglia, V. Galimberti, G. Viale, S. Pece, and P.P. Di Fiore. 2008. NUMB controls p53 tumour suppressor activity. *Nature*. 451:76–80. http://dx.doi.org/10.1038/nature06412

Colnot, S., M. Niwa-Kawakita, G. Hamard, C. Godard, S. Le Plenier, C. Houbron, B. Romagnolo, D. Berrebi, M. Giovannini, and C. Perret. 2004. Colorectal cancers in a new mouse model of familial adenomatous polyposis: influence of genetic and environmental modifiers. *Lab. Invest.* 84:1619–1630. http://dx.doi.org/10.1038/labinvest.3700180

Dho, S.E., M.B. French, S.A. Woods, and C.J. McGlade. 1999. Characterization of four mammalian numb protein isoforms. Identification of cytoplasmic and membrane-associated variants of the phosphotyrosine binding domain. *J. Biol. Chem.* 274:33097–33104. http://dx.doi.org/10.1074/jbc.274.46.33097

Dho, S.E., J. Trejo, D.P. Siderovski, and C.J. McGlade. 2006. Dynamic regulation of mammalian numb by G protein-coupled receptors and protein kinase C activation: Structural determinants of numb association with the cortical membrane. *Mol. Biol. Cell*. 17:4142–4155. http://dx.doi.org/10.1091/mbc.E06-02-0097

Dikovskaya, D., D. Schiffmann, I.P. Newton, A. Oakley, K. Kroboth, O. Sansom, T.J. Jamieson, V. Meniel, A. Clarke, and I.S. Näthke. 2007. Loss of APC induces polyploidy as a result of a combination of defects in mitosis and apoptosis. *J. Cell Biol.* 176:183–195. http://dx.doi.org/10.1083/jcb.200610099

Draviam, V.M., I. Shapiro, B. Aldridge, and P.K. Sorger. 2006. Misorientation and reduced stretching of aligned sister kinetochores promote chromosome missegregation in EB1- or APC-depleted cells. *EMBO J.* 25:2814–2827. http://dx.doi.org/10.1038/sj.emboj.7601168

Fischer, E., E. Legue, A. Doyen, F. Nato, J.F. Nicolas, V. Torres, M. Yaniv, and M. Pontoglio. 2006. Defective planar cell polarity in polycystic kidney disease. *Nat. Genet.* 38:21–23. http://dx.doi.org/10.1038/ng1701

Fleming, E.S., M. Zajac, D.M. Moschenross, D.C. Montrose, D.W. Rosenberg, A.E. Cowan, and J.S. Tirnauer. 2007. Planar spindle orientation and asymmetric cytokinesis in the mouse small intestine. *J. Histochem. Cytochem.* 55:1173–1180. http://dx.doi.org/10.1369/jhc.7A7234.2007

Fleming, E.S., M. Temchin, Q. Wu, L. Maggio-Price, and J.S. Tirnauer. 2009. Spindle misorientation in tumors from APC(min/+) mice. *Mol. Carcinog.* 48:592–598. http://dx.doi.org/10.1002/mc.20506

Fodde, R., R. Smits, N. Hofland, M. Kielman, and P. Meera Khan. 1999. Mechanisms of APC-driven tumorigenesis: lessons from mouse models. *Cytogenet. Cell Genet.* 86:105–111. http://dx.doi.org/10.1159/000015361

Formstone, C.J., C. Moxon, J. Murdoch, P. Little, and I. Mason. 2010. Basal enrichment within neuroepithelia suggests novel function(s) for Celsr1 protein. *Mol. Cell. Neurosci.* 44:210–222. http://dx.doi.org/10.1016/j.mcn.2010.03.008

Fre, S., A. Bardin, S. Robine, and D. Louvard. 2011. Notch signaling in intestinal homeostasis across species: the cases of *Drosophila*, Zebrafish and the mouse. *Exp. Cell Res.* 317:2740–2747. http://dx.doi.org/10.1016/j.yexcr.2011.06.012

Gong, Y., C. Mo, and S.E. Fraser. 2004. Planar cell polarity signalling controls cell division orientation during zebrafish gastrulation. *Nature*. 430:689–693. http://dx.doi.org/10.1038/nature02796

Green, R.A., R. Wollman, and K.B. Kaplan. 2005. APC and EB1 function together in mitosis to regulate spindle dynamics and chromosome alignment. *Mol. Biol. Cell*. 16:4609–4622. http://dx.doi.org/10.1091/mbc.E05-03-0259

Gulino, A., L. Di Marcotullio, and I. Screpanti. 2010. The multiple functions of Numb. *Exp. Cell Res.* 316:900–906. http://dx.doi.org/10.1016/j.yexcr.2009.11.017

Helms, A.W., and J.E. Johnson. 1998. Progenitors of dorsal commissural interneurons are defined by MATH1 expression. *Development*. 125:919–928.

Jory, A., I. Le Roux, B. Gayraud-Morel, P. Rocheteau, M. Cohen-Tannoudji, A. Cumano, and S. Tajbakhsh. 2009. Numb promotes an increase in skeletal muscle progenitor cells in the embryonic somite. *Stem Cells*. 27:2769–2780. http://dx.doi.org/10.1002/stem.220

Klein, A.M., and B.D. Simons. 2011. Universal patterns of stem cell fate in cycling adult tissues. *Development*. 138:3103–3111. http://dx.doi.org/10.1242/dev.060103

Lopez-Garcia, C., A.M. Klein, B.D. Simons, and D.J. Winton. 2010. Intestinal stem cell replacement follows a pattern of neutral drift. *Science*. 330:822–825. http://dx.doi.org/10.1126/science.1196236

Mahmoud, N.N., S.K. Boolbol, R.T. Bilinski, C. Martucci, A. Chadburn, and M.M. Bertagnolli. 1997. Apc gene mutation is associated with a dominant-negative effect upon intestinal cell migration. *Cancer Res.* 57:5045–5050.

Montcouquiol, M., J.M. Jones, and N. Sans. 2008. Detection of planar polarity proteins in mammalian cochlea. *Methods Mol. Biol.* 468:207–219. http://dx.doi.org/10.1007/978-1-59745-249-6_16

Morin, X., and Y. Bellaïche. 2011. Mitotic spindle orientation in asymmetric and symmetric cell divisions during animal development. *Dev. Cell*. 21:102–119. http://dx.doi.org/10.1016/j.devcel.2011.06.012

Neumüller, R.A., and J.A. Knoblich. 2009. Dividing cellular asymmetry: asymmetric cell division and its implications for stem cells and cancer. *Genes Dev.* 23:2675–2699. http://dx.doi.org/10.1101/gad.1850809

Pease, J.C., and J.S. Tirnauer. 2011. Mitotic spindle misorientation in cancer—out of alignment and into the fire. *J. Cell Sci.* 124:1007–1016. http://dx.doi.org/10.1242/jcs.081406

Quyn, A.J., P.L. Appleton, F.A. Carey, R.J. Steele, N. Barker, H. Clevers, R.A. Ridgway, O.J. Sansom, and I.S. Näthke. 2010. Spindle orientation bias in gut epithelial stem cell compartments is lost in precancerous tissue. *Cell Stem Cell*. 6:175–181. http://dx.doi.org/10.1016/j.stem.2009.12.007

Rasin, M.R., V.R. Gazula, J.J. Breunig, K.Y. Kwan, M.B. Johnson, S. Liu-Chen, H.S. Li, L.Y. Jan, Y.N. Jan, P. Rakic, and N. Sestan. 2007. Numb and Numbl are required for maintenance of cadherin-based adhesion and polarity of neural progenitors. *Nat. Neurosci.* 10:819–827. http://dx.doi.org/10.1038/nn1924

Reinsch, S., and E. Karsenti. 1994. Orientation of spindle axis and distribution of plasma membrane proteins during cell division in polarized MDCKII cells. *J. Cell Biol.* 126:1509–1526. http://dx.doi.org/10.1083/jcb.126.6.1509

Rothenberg, M.E., Y. Nusse, T. Kalisky, J.J. Lee, P. Dalerba, F. Scheeren, N. Lobo, S. Kulkarni, S. Sim, D. Qian, et al. 2012. Identification of a cKit(+) colonic crypt base secretory cell that supports Lgr5(+) stem cells in mice. *Gastroenterology*. 142:1195–1205.e6. http://dx.doi.org/10.1053/j.gastro.2012.02.006

Sato, T., J.H. van Es, H.J. Snippert, D.E. Stange, R.G. Vries, M. van den Born, N. Barker, N.F. Shroyer, M. van de Wetering, and H. Clevers. 2011. Paneth cells constitute the niche for Lgr5 stem cells in intestinal crypts. *Nature*. 469:415–418. http://dx.doi.org/10.1038/nature09637

Shroyer, N.F., M.A. Helmrath, V.Y.C. Wang, B. Antalffy, S.J. Henning, and H.Y. Zoghbi. 2007. Intestine-specific ablation of mouse atonal homolog 1 (Math1) reveals a role in cellular homeostasis. *Gastroenterology*. 132:2478–2488. http://dx.doi.org/10.1053/j.gastro.2007.03.047

Simons, B.D., and H. Clevers. 2011. Strategies for homeostatic stem cell self-renewal in adult tissues. *Cell*. 145:851–862. http://dx.doi.org/10.1016/j.cell.2011.05.033

Simons, M., and G. Walz. 2006. Polycystic kidney disease: cell division without a c(l)ue? *Kidney Int.* 70:854–864. http://dx.doi.org/10.1038/sj.ki.5001534

Snippert, H.J., L.G. van der Flier, T. Sato, J.H. van Es, M. van den Born, C. Kroon-Veenboer, N. Barker, A.M. Klein, J. van Rheenen, B.D. Simons, and H. Clevers. 2010. Intestinal crypt homeostasis results from neutral competition between symmetrically dividing Lgr5 stem cells. *Cell*. 143:134–144. http://dx.doi.org/10.1016/j.cell.2010.09.016

Strutt, D. 2005. Organ shape: controlling oriented cell division. *Curr. Biol.* 15:R758–R759. http://dx.doi.org/10.1016/j.cub.2005.08.053

Su, L.K., K.W. Kinzler, B. Vogelstein, A.C. Preisinger, A.R. Moser, C. Luongo, K.A. Gould, and W.F. Dove. 1992. Multiple intestinal neoplasia caused by a mutation in the murine homolog of the APC gene. *Science*. 256:668–670. http://dx.doi.org/10.1126/science.1350108

van Es, J.H., P. Jay, A. Gregorieff, M.E. van Gijn, S. Jonkheer, P. Hatzis, A. Thiele, M. van den Born, H. Begthel, T. Brabletz, et al. 2005. Wnt signalling induces maturation of Paneth cells in intestinal crypts. *Nat. Cell Biol.* 7:381–386. http://dx.doi.org/10.1038/ncb1240

Wasan, H.S., H.S. Park, K.C. Liu, N.K. Mandir, A. Winnett, P. Sasieni, W.F. Bodmer, R.A. Goodlad, and N.A. Wright. 1998. APC in the regulation of intestinal crypt fission. *J. Pathol.* 185:246–255. http://dx.doi.org/10.1002/(SICI)1096-9896(199807)185:3<246::AID-PATH90>3.0.CO;2-8

Yang, Q., N.A. Bermingham, M.J. Finegold, and H.Y. Zoghbi. 2001. Requirement of Math1 for secretory cell lineage commitment in the mouse intestine. *Science*. 294:2155–2158. http://dx.doi.org/10.1126/science.1065718

Zhong, W., J.N. Feder, M.M. Jiang, L.Y. Jan, and Y.N. Jan. 1996. Asymmetric localization of a mammalian numb homolog during mouse cortical neurogenesis. *Neuron.* 17:43–53. http://dx.doi.org/10.1016/S0896-6273(00)80279-2